Available online at www.sciencedirect.com
ScienceDirect
Journal of Catalysis 250 (2007) 331–341
JOURNAL OF CATALYSIS
www.elsevier.com/locate/jcat

Deactivation of Ni catalysts during methane autothermal reforming with CO_2 and O_2 in a fluidized-bed reactor

Zhaoyin Hou *, Jing Gao, Jianzhong Guo, Dan Liang, Hui Lou, Xiaoming Zheng

Institute of Catalysis, Department of Chemistry, Zhejiang University (xixi campus) Hangzhou 310028, China

Received 28 March 2007; revised 22 June 2007; accepted 27 June 2007

Available online 7 August 2007

Abstract

A series of different-sized Ni catalysts (4.5–45.0 nm) were prepared and used for methane autothermal reforming with CO_2 and O_2 in a fluidized-bed reactor. It was found that the activity and stability of Ni catalysts depend strongly on the particle size and the operating space velocity. Small sized Ni is more active and stable at space velocity $<54{,}000\ h^{-1}$. Characterizations disclosed that methane decomposition rate decreases with the enlarging Ni particle size, and some of the surface carbons (derived from methane decomposition) are inactive in CO_2 atmosphere. As the methane decomposition rate slows on larger Ni particles and at higher space velocity to ensure complete conversion of the oxygen, surface Ni will be gradually oxidized by remaining O_2, leading to Ni deactivation.

Keywords: Methane; Reforming; Ni catalyst; Deactivation; Space velocity

1. Introduction

The transformation of methane and carbon dioxide, the cheapest carbon-containing materials and the most problematic greenhouse gases, into more valuable compounds has long attracted the attention of researchers. Among published results, the catalytic CO_2 reforming of CH_4 to synthesis gas [Eq. (1)] has been investigated comprehensively over the past few years, as has been well summarized in recent reviews [1–5]. The synthesis gas generated from CO_2 reforming of CH_4 has a low H_2/CO ratio and thus is suitable for the Fischer–Tropsch synthesis of higher hydrocarbons and for the synthesis of oxygenate products. Rostrup–Nielsen's group [6,7] and Ruckenstein's group [1,5,8] have made significant contributions to improving the understanding of steam and CO_2 reforming over Ni catalysts in both experimental research and theoretical studies:

$$CH_4 + CO_2 \rightarrow 2CO + 2H_2, \quad \Delta H_{298K} = 247\ \text{kJ/mol}. \qquad (1)$$

Most of the group VIII metals are more or less active toward this reaction, and Ni has been popularly explored for its high activity and low price [1–5,9]. Due to the inherent inertness of methane and CO_2, high temperature (typically, 800–900 °C) is needed to achieve a meaningful yield. Under such severe conditions, carbon deposition and/or sintering of the metal particles occur on the surface of the catalyst, and sintering further accelerates carbon deposition because large metal ensembles stimulate coke formation [8].

Another drawback is that CO_2 reforming of methane is a highly endothermic reaction (247 kJ/mol). The addition of oxygen to the reforming reactants is an effective method of supplying heat, because partial oxidation of methane to synthesis gas is an exothermic reaction [Eq. (2)]. This combined CO_2 reforming and partial oxidation of methane, also called methane autothermal reforming [MATR], has drawn significant interest in recent years in alternative routes for the conversion of methane to synthesis gas [Eq. (3)] [10–16]:

$$CH_4 + (1/2)O_2 \rightarrow CO + 2H_2, \quad \Delta H_{298K} = -38\ \text{kJ/mol}, \qquad (2)$$

$$CH_4 + xCO_2 + ((1-x)/2)O_2 \rightarrow CO + 2H_2, \quad \Delta H_{298K} = (285x - 38)\ \text{kJ/mol} \quad (0 < x < 1). \qquad (3)$$

In published papers, it is suggested that MATR is carried out in two separate reaction zones in the fixed-bed reactor—in the first zone, part methane is combusted into CO_2 and steam to en-

* Corresponding author. Fax: +86 571 88273283.
E-mail address: zyhou@zju.edu.cn (Z. Hou).

0021-9517/$ – see front matter
doi:10.1016/j.jcat.2007.06.023

sure the complete conversion of the oxygen in feed, producing a hot (>1300 °C) stream, and in the second zone, the unconverted methane is reformed to synthesis gas by CO_2 and steam. A significant temperature gradient in the catalyst bed formed, which ultimately resulted in the thermal sintering and deactivation of catalyst [10,17,18]. It is of great practical interest to overcome this limitation of the MATR process in fixed-bed reactor.

Tomishige [11–13] and Zheng [15,19,20] reported their studies on the MATR process in a fluidized-bed reactor, and they suggested that the high rates of heat transfer and high stability of operation be obtained. Fluidization has a favorable effect on the inhibition of carbon deposition, which is probably because the catalyst particles are circulated between the oxidizing zone and reducing zone and carbon gasification proceeds readily in the oxidizing zone. Moreover, catalyst can maintain a suitable level of reducibility during fluidization that enhances the conversion of methane [11–13,15,19,20].

Recently, we have found that the activity and stability of Ni catalysts during the MATR in fluidized-bed reactor depend strongly on the particle size of Ni and the operating space velocity. Larger-sized Ni catalysts (average Ni particle size >16 nm) are inactive at higher space velocity (90,000 h^{-1}) and deactivate rapidly (at low space velocity, 18,000 h^{-1}). Whereas small-sized ones (average Ni particle <9.5 nm) are more active and stable at the space velocity <54,000 h^{-1}. Characterizations of the spent catalysts have found that neither carbon deposition nor metal sintering would form on the deactivated catalysts. That is, the deactivation mechanism of Ni catalysts during the MATR process in a fluidized-bed reactor cannot be explained by those achievements of CO_2 reforming of methane. More fundamental studies are still needed to reveal the deactivation mechanism of Ni catalyst in the MATR process in the fluidized-bed reactor. The aim of this work is to correlate the particle size of Ni and the operating space velocity with its catalytic performance and deactivation. For this purpose, MATR at different space velocities, methane decomposition (in both continuous and pulsed methane flow) and the reactivity of carbon deposited during methane decomposition toward CO_2 and O_2 were determined on different-sized Ni catalysts.

2. Experimental

2.1. Catalyst preparation and characterizations

Ni catalysts sized from 4.5 to 45.0 nm were prepared via direct impregnation of $[Ni(en)_3]^{2+}$ (en, ethylenediamine), $[Ni(EDTA)]^{2-}$ (EDTA; ethylenediaminetetraacetic acid), nickel(II) acetylacetonate dihydrate (99+%), nickel(II) acetate, and $Ni(NO_3)_2{\cdot}6H_2O$ onto a spherical SiO_2 support (special product for fluidized reactor, $S_{BET} = 330\ m^2\ g^{-1}$, average diameter 0.25–0.38 mm, Qingdao, China). Nickel(II) acetylacetonate dihydrate (99+%), nickel(II) acetate, and $Ni(NO_3)_2{\cdot}6H_2O$ were purchased from Acros Organics (Beijing Branch, China). $[Ni(en)_3]^{2+}$ and $[Ni(EDTA)]^{2-}$ were prepared as described previously [21–23]. The loading amount of Ni was controlled at 5 wt% of the support. The precursors were dried at 80 °C in vacuum and calcined at 800 °C in stagnant air for 4 h.

The morphologies of these catalysts were characterized by X-ray diffraction (XRD) and transmission electron microscopy (TEM). XRD was obtained in D8 Advance (Bruker, Germany) equipment using nickel-filtered Cu$K\alpha$ radiation at 40 kV and 40 mA. Diffraction data were recorded using continuous scanning at a rate of 0.02°/s, step 0.02°. Average Ni particle size was calculated according to Scherrer–Warren equation. TEM images were obtained using an accelerating voltage of 200 kV (TEM, JEOL-2020F). Samples were first ground to powder, reduced in hydrogen, and dispersed on Cu grids in tetrachloromethane under supersonic-wave shaking.

2.2. MATR on different-sized Ni catalysts

MATR was carried out in a quartz fluidized-bed reactor (id = 12 mm). As noted previously [24], the minimum fluidization velocity (ω_{mf}) and the maximum fluidization velocity (ω_t) could be calculated as

$$\omega_{mf} = \frac{d_p^2(r_s - r_g)g}{1650\mu_g}\ (\mathrm{m/s}) \tag{4}$$

and

$$\omega_t = \frac{d_p^2(r_s - r_g)g}{18\mu_g}\ (\mathrm{m/s}), \tag{5}$$

where d_p and r_s are the diameter and the density of catalyst, and μ_g and r_g are the viscosity and density of the reactant mixture. In this experiment ($d_p = 0.25$–0.38 mm, $r_s = 470$–$500\ kg/m^3$, $r_g = 0.32\ kg/m^3$ and $\mu_g = 37.5\ \mu Pa/s$), the total feed gas flow rate must be controlled between 78 and 3070 ml/min to ensure the efficient fluidization of catalysts particles in the reactor at 700 °C.

CH_4 (99.99%), CO_2 (99.9%), and O_2 (99.9%) were introduced into the reactor controlled by three sets of mass flow controller (Brooks 5850E) at a molar ratio of CH_4:CO_2:O_2 = 10:4:3. Catalyst is first reduced in H_2 at 700 °C for 1 h. The effluent gas was cooled in an ice-water trap and analyzed using an online gas chromatograph (Shimadzu, GC-8A) with a packed column (TDX-01) and a thermal conductivity detector. All spent catalysts were further characterized by XRD and TG-DTA (PE-TGA7) at 50–900 °C in air flow.

2.3. The reactivity of surface carbons on different-sized Ni catalysts

The reactivity of surface carbons toward CO_2 and O_2 was investigated via coking reaction (CH_4 temperature-programmed decomposition [CH_4-TPDe]) and followed temperature-programmed oxidation with CO_2 (CO_2-TPO) and O_2-TPO. Before these experiments, catalysts were first reduced in H_2 flow at 700 °C for 1 h, then cooled to 50 °C in Ar. CH_4-TPDe was performed in 10% CH_4/Ar (50 ml/min) from 50 to 800 °C at a ramp of 15 °C/min and held at 800 °C for 20 min. Then the catalyst bed was cooled to 50 °C in Ar, and CO_2-TPO was performed in 10% CO_2/Ar (50 ml/min) from 50 to 800 °C at a ramp of 15 °C/min. Finally, after the catalyst bed was cooled to 50 °C in Ar, consecutive O_2-TPO was carried out in a flow

of 10% O_2/Ar (50 ml/min) from 50 to 800 °C at 15 °C/min. All gases in effluent were detected by a mass analyzer (OmniStar GSD301, Switzerland) and recorded as functions of temperature. Parallel experiments were performed simultaneously, and carbons formed in CH_4-TPD and residual carbons after CO_2-TPO were detected by TG-DTA from 50 to 900 °C in air flow. The morphologies of the surface carbons (formed in CH_4-TPDe) were characterized by TEM.

2.4. Methane activation on different-sized Ni catalysts

Methane activation and catalytic conversion on different-sized Ni catalysts in various atmospheres (CH_4, CH_4/CO_2, and CH_4/O_2) were investigated via pulse-injected surface reaction. CH_4, CH_4/O_2 (2:1), or CH_4/CO_2 (1:1) pulse (total volume, 500 μL with 250 μL CH_4 and Ar in balance) was injected into the reduced catalysts (20 mg) with a 6-port gas sampling valve under a stream of Ar carrier gas (100 mL/min). The reaction temperature was kept at 700 °C. All gases in effluent were detected, the turnover frequency of methane (TOF, defined as mol of CH_4 converted/mol of Ni atom per second) was calculated on the basis of methane conversion.

2.5. Reducibility of different-sized Ni catalysts after CH_4 decomposition

The reducibility of different-sized Ni catalysts was detected via consecutive CH_4–O_2–H_2 pulse experiments in the same equipment as described in Section 2.3. Six methane pulses (250 μL per pulse) were first injected into the reduced catalyst (20 mg), followed by three oxygen pulses, and then hydrogen pulses in a stream of Ar carrier gas (100 mL/min). The reaction temperature was kept at 700 °C, and all gases in effluent were recorded.

3. Results

3.1. The dimensions of Ni on SiO_2

Table 1 summarizes the TEM and XRD analysis results of the Ni/SiO_2 catalysts prepared from different Ni precursors. The mean size of nickel crystallites was detected by XRD and calculated from the broadening of the Ni(111) according to the Scherrer–Warren equation. The calculated average Ni particle sizes increased from 4.5 to 45.0 nm in these Ni/SiO_2 catalysts prepared via $[Ni(en)_3]^{2+}$ and nickel nitrate. In the Ni/SiO_2 catalysts prepared from $[Ni(EDTA)]^{2-}$, nickel(II) acetylacetonate, and nickel(II) acetate, the calculated average Ni particle sizes were 6.0, 8.5, and 16.0 nm, respectively.

Figs. 1A–1E show the typical TEM images of Ni/SiO_2 catalysts prepared from $[Ni(en)_3]^{2+}$, $[Ni(EDTA)]^{2-}$, nickel(II) acetylacetonate, nickel(II) acetate, and nickel nitrate. The histograms of the particle size distribution are inserted in the top-right corner of the TEM images. Highly dispersed Ni particles were detected in those Ni/SiO_2 catalysts prepared from $[Ni(en)_3]^{2+}$ and $[Ni(EDTA)]^{2-}$, and the detected Ni particles were concentrated at 5.1 and 7.0 nm, respectively. The average

Table 1
The dimensions of Ni on SiO_2 from different Ni precursors[a]

Ni precursors	Ni diameter (nm)	
	TEM	XRD[b]
Aqueous solution of $[Ni(en)_3]^{2+}$	5.1	4.5
Aqueous solution of $[Ni(EDTA)]^{2-}$	7.0	6.0
Ethanol solution of nickel(II) acetylacetonate	9.4	8.5
Aqueous solution of nickel(II) acetate	16.1	16.0
Aqueous solution of $Ni(NO_3)_2$	51.2	45.0

[a] Sample was reduced in H_2 at 700 °C for 1 h.
[b] Calculated according to Scherrer–Warren equation.

particle size of Ni (summarized in Table 1) was calculated as

$$d_{\mathrm{TEM}} = \frac{\sum n_i d_i^3}{\sum n_i d_i^2}, \tag{6}$$

where n_i is the number of particles having a characteristic diameter d_i (within a given diameter range).

In Ni/SiO_2 catalysts prepared from nickel(II) acetate and nickel nitrate, a lower density of Ni particles on the support should be expected. However, the silica support appeared to be almost completely covered by Ni particles (Fig. 1D), suggesting that the Ni could be unevenly distributed within the silica spheres, with some parts heavily loaded with Ni and others bearing only few Ni particles.

3.2. MATR on different-sized Ni catalysts

Fig. 2 shows the activity of different-sized Ni/SiO_2 catalysts for MATR in fluidized-bed reactor at 700 °C and a space velocity of 18,000 h^{-1}. The detected conversions of CH_4 and CO_2 were higher and more stable on the smaller-particle Ni catalysts (<9.5 nm) than that on the larger-particle ones (>16 nm). Moreover, the oxygen in the feed was consumed completely on the smaller-particle Ni catalysts. The highest CH_4 and CO_2 conversions were 77.0 and 67.9%, respectively. But on the 45.0-nm Ni catalyst, the initial conversions of CH_4 and CO_2 were only 47.2 and 27.5%, and the catalyst deactivated rapidly. The residual oxygen in effluent increased during the deactivation process.

At higher space velocity (54,000 h^{-1}), the detected conversion of methane on 4.5-nm Ni catalyst decreased rapidly from 71.0 to 66.4% in the first 4 h and remained constant in the following 38 h (Fig. 3). But the 45.0-nm Ni catalyst deactivated completely in only 2 h. When the space velocity was enhanced to 90,000 h^{-1}, the detected conversion of methane on the 4.5-nm Ni catalyst decreased continuously from 67.2 to 37.2% in 48 h on stream, and the 45.0-nm Ni catalyst was inactive at this space velocity.

Fig. 4 shows the durability of the 4.5-nm Ni catalyst for MATR in a fluidized-bed reactor at lower space velocity. It remained stable during 100 h on stream (at 9000 h^{-1}), with the detected conversion of CH_4 decreasing only slightly, from 81.3 to 80.8%. At 18,000 h^{-1}, the detected conversion of CH_4 decreased from 77.0 to 70.0% in the first 26 h, but it recovered in the following 16 h and remained stable (72.0%) for the last 38 h.

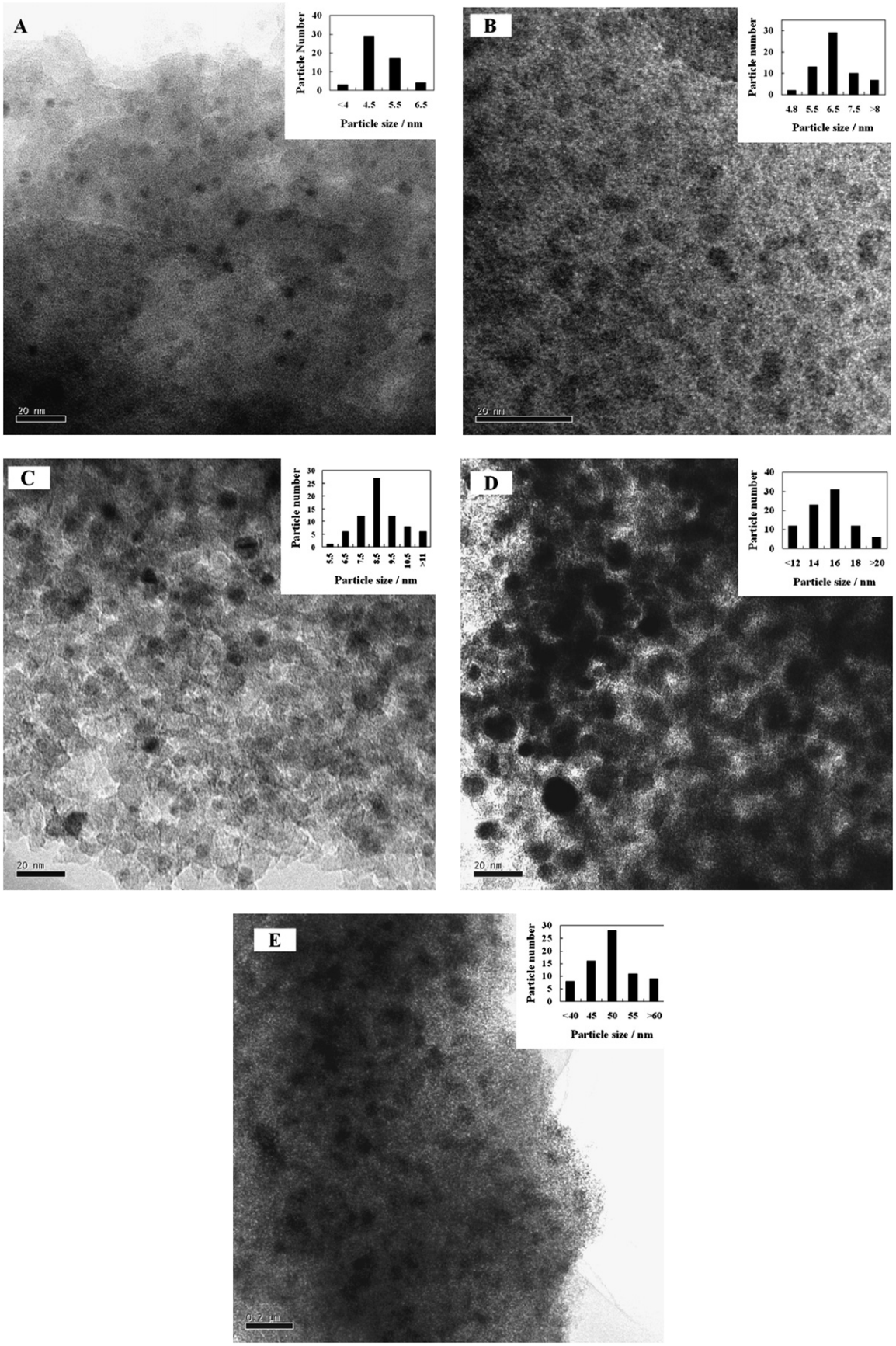

Fig. 1. TEM image and particle distribution of Ni/SiO_2 catalysts prepared from different Ni precursors: (A) $[Ni(en)_3]^{2+}$, (B) $[Ni(EDTA)]^{2-}$, (C) nickel(II) acetylacetonate, (D) nickel(II) acetate, and (E) $Ni(NO_3)_2$.

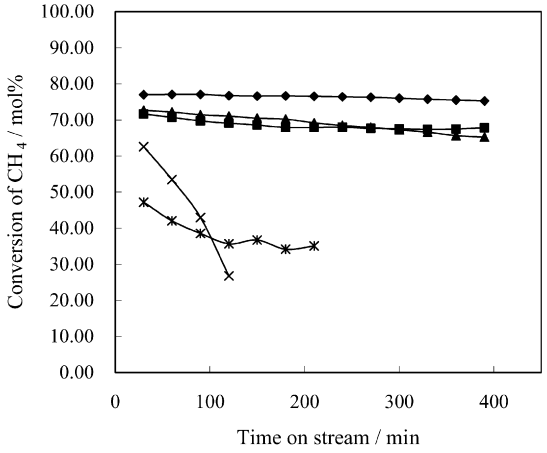

Fig. 2. Activity of the different sized Ni catalysts for MATR in fluidized bed reactor at 18,000 h^{-1}: (◆) 4.5, (■) 6.0, (▲) 8.5, (×) 16.0, and (✳) 45.0 nm.

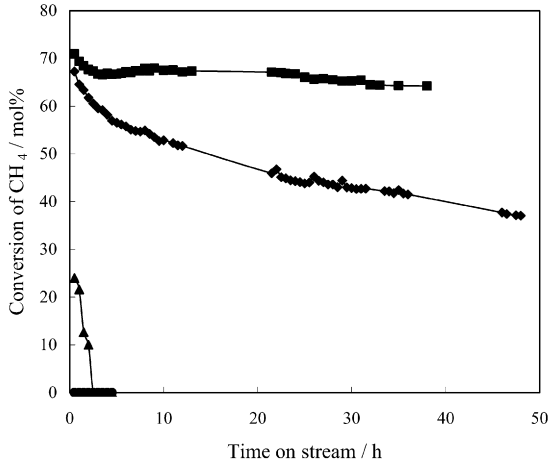

Fig. 3. Activity of 4.5 nm and 45.0 nm sized Ni catalysts at higher space velocity: (■) and (◆) 4.5 nm sized Ni at 54,000 and 90,000 h^{-1}, (▲) and (●) 45.0 nm sized Ni at 54,000 and 90,000 h^{-1}.

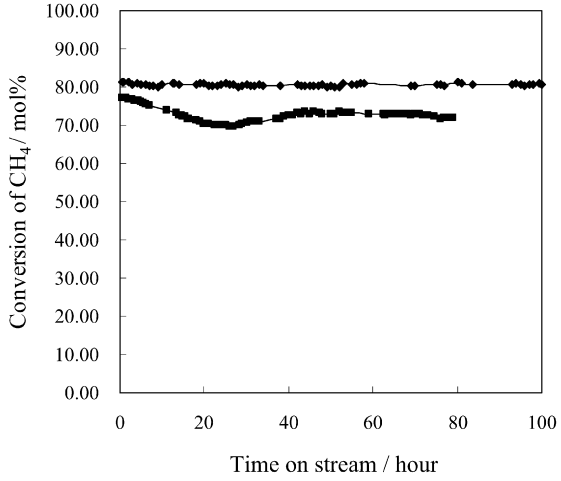

Fig. 4. The durability of the 4.5 nm sized Ni catalyst for MATR in fluidized bed reactor: (◆) 9000 and (■) 18,000 h^{-1}.

TG-DTA and XRD analysis of the spent catalysts found that neither carbon deposition nor metal sintering formed. Ni was in high dispersion and metallic state in the spent 4.5-nm catalyst as

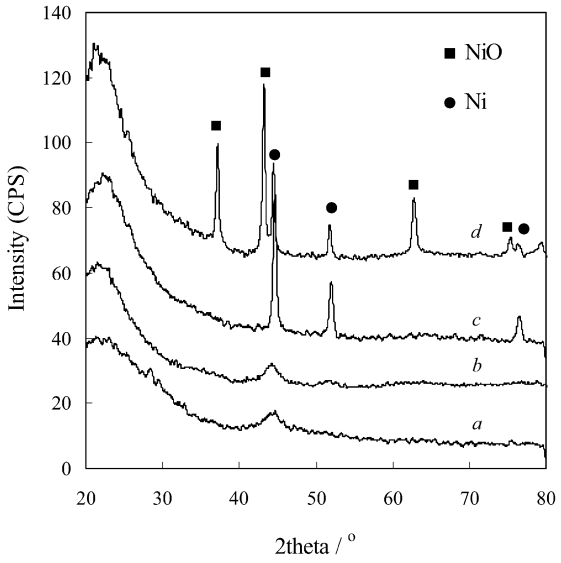

Fig. 5. XRD spectrum of different sized Ni catalysts: (a) 4.5 nm fresh, (b) 4.5 nm spent (6 h), (c) 45.0 nm fresh, and (d) 45.0 nm spent (6 h).

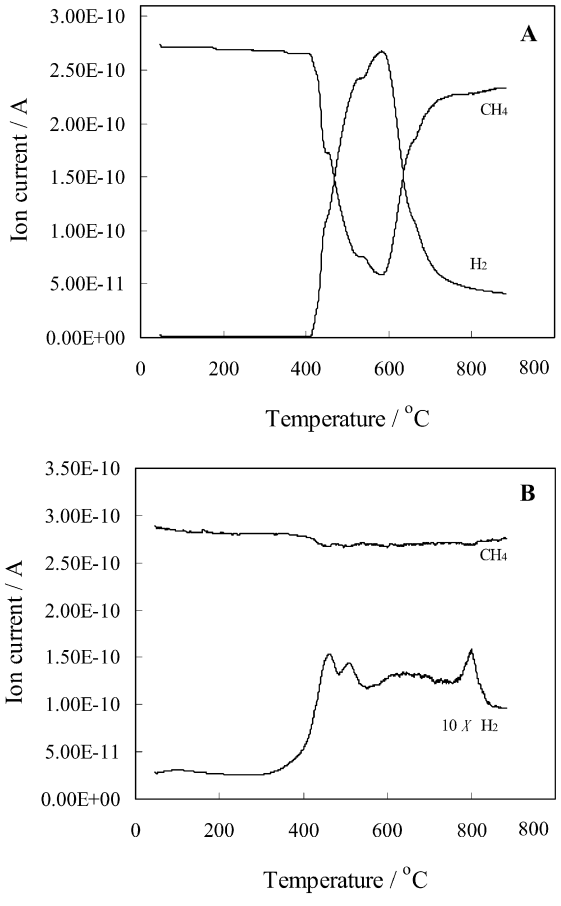

Fig. 6. MS signals of effluent gases during CH_4-TPDe: (a) on the 45.0 nm sized Ni catalyst and (B) on the 4.5 nm sized Ni catalyst.

that in the fresh sample. But NiO obviously formed in the spent 45.0-nm Ni catalyst (Fig. 5), suggesting that Ni was oxidized during time on stream. This might be the direct reason for the deactivation of the larger-particle Ni catalysts.

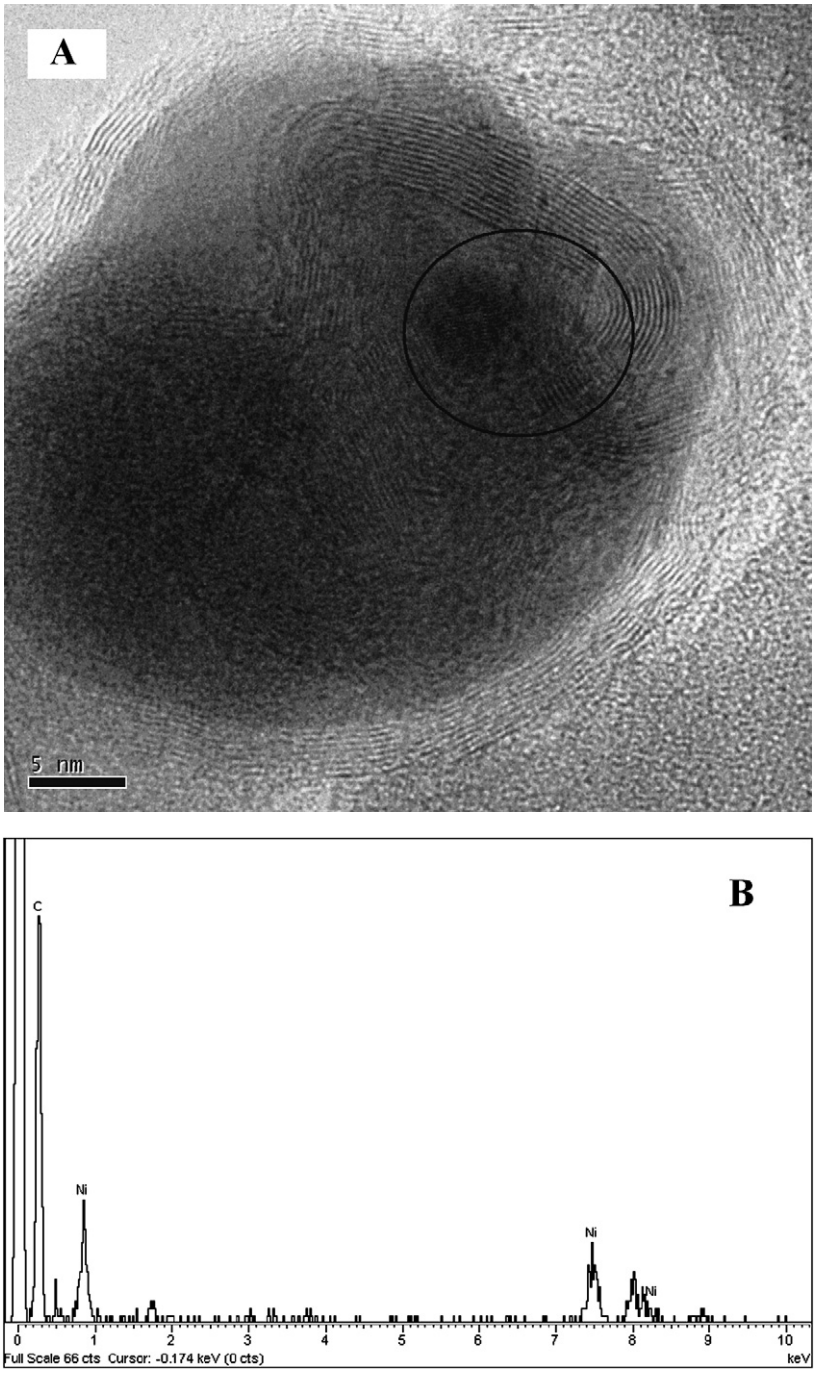

Fig. 7. TEM and EDX analysis of the 45.0 nm sized Ni catalyst after CH_4-TPDe: (A) TEM image and (B) EDX analysis (in circle). Spectrum processing: no peaks omitted; quantization method: cliff lorimer thin ratio section; processing option: all elements analyzed (normalised), number of iterations = 1.

3.3. The reactivity of surface carbons on different-sized Ni catalysts

Figs. 6A and 6B show the typical MS signals of effluent gases during the coke reaction via CH_4-TPDe on the 45.0- and 4.5-nm Ni catalysts, respectively. Three CH_4 decomposition peaks can be seen at 410–800 °C on the 45.0-nm Ni catalyst, and four peaks can be seen at 370–800 °C on the 4.5-nm Ni catalyst. These peaks can be assigned to different kinds of carbons formed as described in earlier work [25]. It is interesting to note that the initial CH_4 decomposition temperature decreased from 410 °C (on the 45.0-nm Ni catalyst) to 370 °C (on the 4.5-nm Ni catalyst), and the amount of deposited carbons decreased from 12.9 to 1.7 mmol/g_{cat} (Table 2).

TEM images and EDX analysis of the carbon-covered Ni catalysts are shown in Figs. 7 and 8. Large amounts of encapsulating carbon and whisker carbon [26–28] formed on the 45.0-nm Ni catalyst, completely enwrapping the Ni particles (Fig. 7A). EDX analysis (in the circled area) of the enwrapped Ni particles found that the surface C/Ni ratio reached 96.3/3.7 (Fig. 7B). In contrast, the 4.5-nm Ni catalyst showed high dispersion (Fig. 8A), with a surface C/Ni ratio of 9.6/2.1 (Fig. 8B).

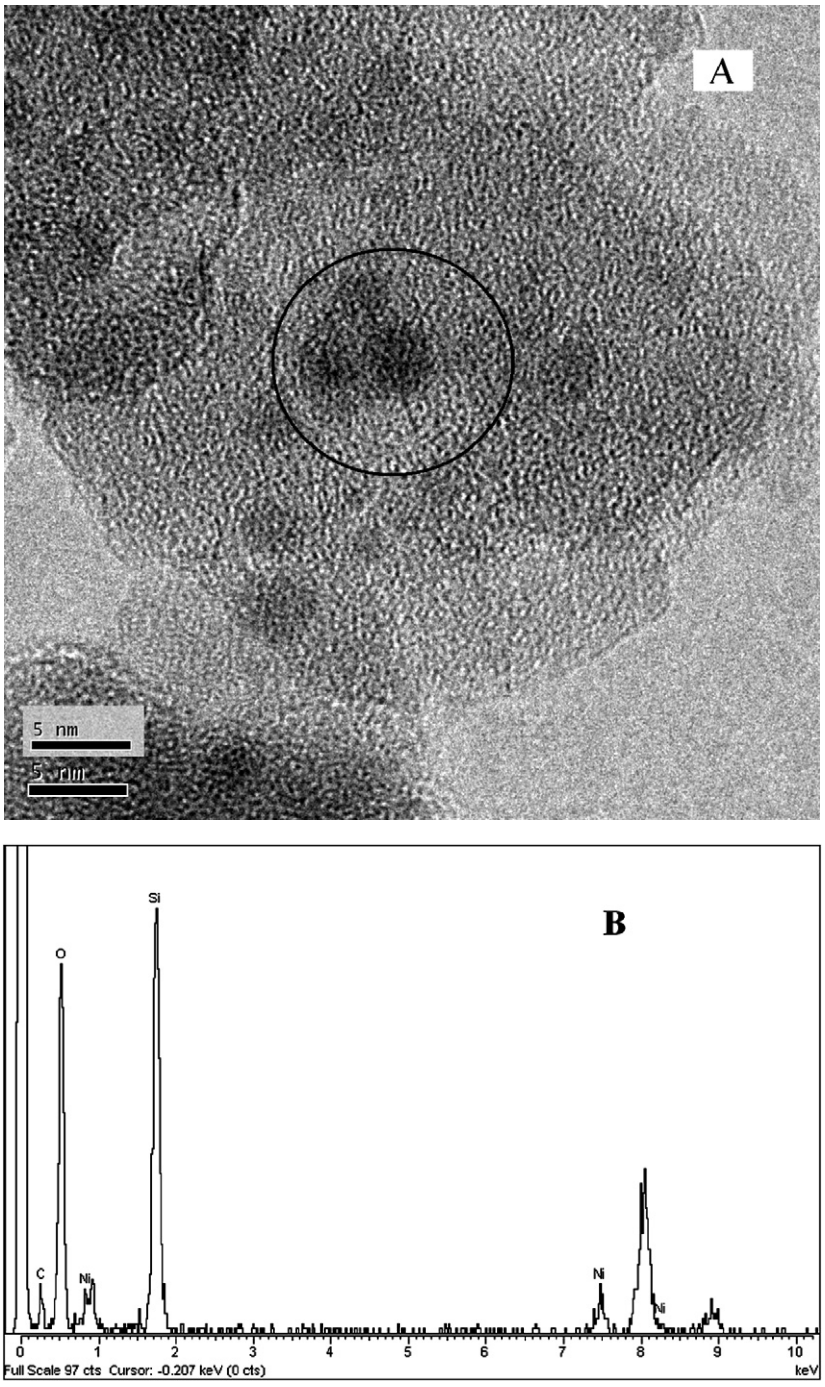

Fig. 8. TEM and EDX analysis of the 4.5 nm sized Ni catalyst after CH_4-TPDe: (A) TEM image and (B) EDX analysis (in circle). Spectrum processing: peak possibly omitted: 8.895 keV; quantization method: cliff lorimer thin ratio section; processing option: all elements analyzed (normalised), number of iterations = 1.

Table 2
The amount of carbon on the 45.0 nm and the 4.5 nm sized Ni catalysts

Catalyst	Carbon ($mmol/g_{cat}$)		
	Total	Removed by CO_2	Inactive carbon
45.0 nm	12.9	10.4	2.5
4.5 nm	1.7	1.3	0.4

The reactivity of the deposited carbons on different-sized Ni catalysts during CH_4-TPDe was investigated via consecutive CO_2-TPO and O_2-TPO (Figs. 9 and 10). In the effluent of CO_2-TPO, CO (formed via the gasification of surface carbons by CO_2) was detected at 500 °C. On the 45.0-nm Ni catalyst, the detected CO reached a maximum at 736 °C, and 10.4 $mmol/g_{cat}$ deposited carbons in CH_4-TPDe were removed by CO_2 (as confirmed by TG analysis of CO_2-TPO spent catalyst). But on the small-particle Ni catalysts (<16 nm), CO in effluent reached its maximum at 590 °C and the amount of the produced CO decreased continuously thereafter with decreasing Ni particle size. On the 4.5-nm Ni catalyst, 1.3 $mmol/g_{cat}$ carbons were removed by CO_2 (Table 2).

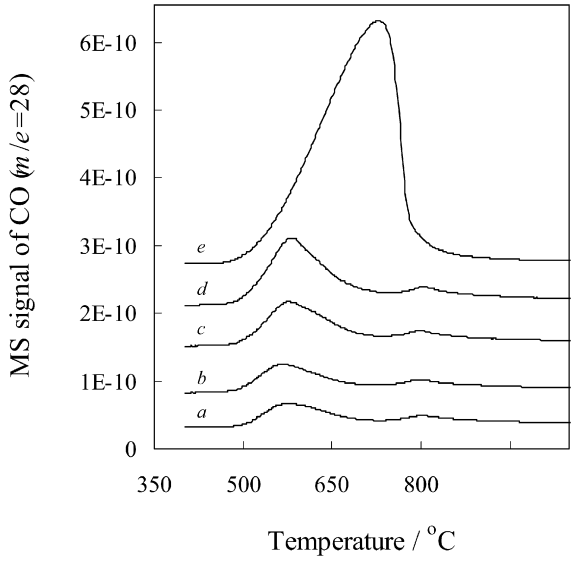

Fig. 9. The reactivity of carbons (formed in CH_4-TPDe) towards CO_2 on the different sized Ni catalysts: (a) 4.5, (b) 6.0, (c) 8.5, (d) 16.0, and (e) 45.0 nm.

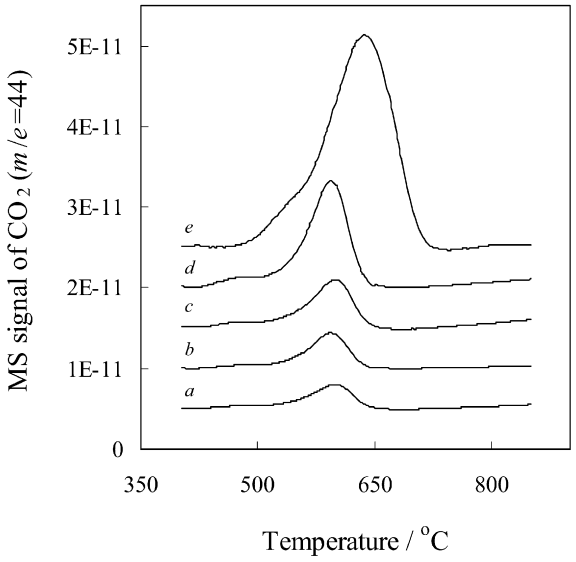

Fig. 10. The reactivity of residual carbons (after CO_2-TPO) towards O_2 on the different sized Ni catalysts: (a) 4.5, (b) 6.0, (c) 8.5, (d) 16.0, and (e) 45.0 nm.

It was surprising to find that carbons formed in CH_4-TPDe cannot be removed completely by CO_2 (even at 800 °C for 20 min). CO_2 (formed via the reaction between the remaining carbons with O_2) was detected (Fig. 10) in the consecutive O_2-TPO, suggesting that this carbon was inactive in CO_2 atmosphere. The amount of inactive carbon decreased from 2.5 mmol/g_{cat} on the 45.0-nm Ni catalyst to 0.4 mmol/g_{cat} on the 4.5-nm Ni catalyst. These kinds of inactive carbons would accumulate and cause a heavy carbon deposition, which is a main drawback of the dry reforming process [26]. In this respect, O_2 in feed is very important in solving the complete loss of catalyst activity (due to carbon deposition) of CO_2 reforming of CH_4.

Table 3
Methane turnover frequency (TOF) in different atmosphere (700 °C)

Pulse No.	Catalyst					
	CH_4 decomposition (TOF (s^{-1}))		CH_4–CO_2 (TOF (s^{-1}))		CH_4–O_2 (TOF (s^{-1}))	
	45.0 nm	4.5 nm	45.0 nm	4.5 nm	45.0 nm	4.5 nm
1	9.8	12.6	15.6	20.6	16.4	22.5
2	7.6	9.6	15.2	20.3	15.8	22.4
3	7.0	9.5	12.1	21.2	15.4	23.0
4	6.8	8.8	11.3	20.7	15.4	22.4
5	6.3	7.4	11.4	21.3	12.0	22.4

3.4. Methane activation and catalytic conversion on different-sized Ni catalysts

Methane activation and catalytic conversion on the 45.0 and 4.5-nm Ni catalysts in various atmospheres (CH_4, CH_4–O_2, and CH_4–CO_2) were investigated via pulse-injected surface reactions. The calculated TOFs of methane are summarized in Table 3. In methane decomposition (with only CH_4 injected), the calculated TOF of methane was 9.8 s^{-1} on the 45.0-nm Ni catalyst, comparable with previously reported values [9]. On the 4.5-nm Ni catalyst, the calculated TOF of CH_4 increased to 12.6 s^{-1}. These data demonstrate that the small-particle Ni catalyst was more active for methane decomposition. With the addition of CO_2 and O_2 in the feed, the detected TOF of CH_4 was greatly enhanced compared with the separated CH_4 decomposition. In CH_4–CO_2 atmosphere, the TOF of CH_4 increased to 20.6 s^{-1} on the 4.5-nm Ni catalyst and remained stable during the first 5 pulses. On the 45.0-nm Ni catalyst, the initial TOF of methane was 15.6 s^{-1}, but decreased continuously with the pulse number. In CH_4–O_2 atmosphere, the TOF of methane further increased to 22.5 s^{-1} on the 4.5-nm Ni catalyst and to 16.4 s^{-1} on the 45.0-nm Ni catalysts. The calculated TOF of methane decreased with the pulse number only on the 45.0-nm Ni catalyst. These results indicate that both CO_2 and O_2 accelerated the conversion of methane, but the small-particle Ni catalyst was more effective and stable.

3.5. Reducibility of different-sized Ni catalysts in MATR

Fig. 11 illustrates the MS spectrum of the consecutive CH_4–O_2–H_2 pulse experiment on the 4.5 and 45.0-nm Ni catalysts. In the first six methane pulses, the residual methane increased with the pulse number. In the subsequent O_2 pulse, no residual oxygen was detected in effluent; H_2O did not form on the 4.5 or the 45.0-nm Ni catalyst, suggesting that mainly carbon (not CH_x) deposited during methane decomposition. Moreover, the amount of CO formed on the 45.0-nm Ni catalyst decreased quickly (Fig. 11A). In the consecutive H_2 pulse, H_2 was obviously consumed, and a large amount of H_2O was detected simultaneously (in the effluent of the 45.0-nm Ni catalyst). H_2O formation could be derived from the reaction between H_2 and Ni oxide. These results indicate that part of the metallic Ni was oxidized during the O_2 pulse because of an insufficient amount of carbon formed in the foregoing CH_4 decomposition; however, on the surface of the 4.5 nm sized Ni catalyst, a large

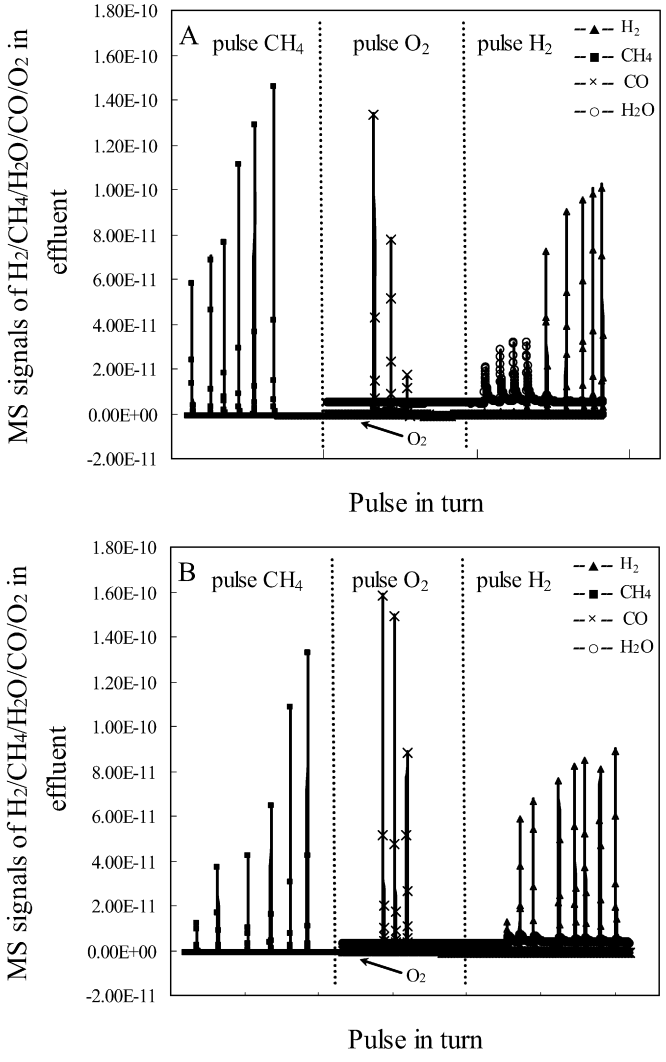

Fig. 11. MS spectrum of the consecutive CH_4–O_2–H_2 pulse: (A) on the 45.0 nm sized Ni catalyst and (B) on the 4.5 nm sized Ni catalyst.

amount of CO was formed, and H_2 consumption and H_2O release were limited (Fig. 11B).

4. Discussion

4.1. Deactivation of Ni catalysts during MATR

MATR, the combined CO_2 reforming and partial oxidation of methane, is of great interest in the conversion of natural gas to synthesis gas for its lower energy requirements due to the opposite contributions of exothermic methane oxidation and endothermic CO_2 reforming [10–20]. And fluidized-bed reactor is recommended for performing this combined reaction efficiently due to its high heat transfer rate and high operational stability.

Our findings indicate that the activity and stability of the Ni catalysts depended strongly on the Ni particle size and the operating space velocity in the fluidized-bed reactor. On the 4.5-nm Ni catalyst, the best conversion of 77.0% of CH_4 and 67.9% of CO_2 at 18,000 h^{-1}. But on the 45.0-nm Ni catalyst, the conversions were only 47.2% of CH_4 and 27.5% of CO_2 (Fig. 2). The 4.5-nm Ni catalyst exhibited high stability at a relatively higher space velocity (<54,000 h^{-1}). On the other hand, the larger-particle Ni catalysts (>16 nm) deactivated rapidly.

Unlike methane dry reforming with CO_2, the deactivation of the larger-particle Ni catalyst was not caused by carbon deposition or sintering of the metal particles. XRD analysis of the spent catalysts (Fig. 5) indicates that the smaller-particle Ni catalyst maintained a high dispersion state as a fresh sample (Fig. 1A), but NiO obviously formed in the spent 45.0-nm Ni catalyst (Fig. 5). These results indicate that large Ni particles are less active than small ones and do not ensure complete conversion of the oxygen added in the feed, leading to Ni oxidation.

4.2. Promotion effect of oxygen in feed

It was surprising to find that part of the carbon (derived from methane decomposition) was inactive in CO_2 atmosphere even at higher temperatures and longer contact times (800 °C for 20 min). This kind of inactive carbon forms on Ni catalyst of any particle size and accumulates and causes carbon deposition, a main drawback of the dry reforming process [26–31]. For this reason, O_2 in feed in the MATR process is very important in solving the complete loss of catalyst activity (due to carbon deposition) of CH_4 dry reforming. The addition of oxygen to the reforming reactants is not only an effective method of providing a heat supply, but also a very important way to avoid catalyst deactivation by carbon deposition. But oxygen in feed has a negative influence at higher space velocity on the larger-particle Ni catalysts in the oxidation of metallic nickel to NiO, causing catalyst deactivation, because of the lower methane decomposition rate on the larger Ni particles.

4.3. Methane decomposition on different-sized Ni catalysts

Numerous mechanistic studies have suggested that during the CH_4 dry reforming and partial oxidation to synthesis gas, CH_4 is decomposed to reactivate carbon species (CH_x, $x = 0$–3) on the metallic sites, which are further oxidized to CO by the oxygen-containing species that originate from CO_2 and O_2 [1–9]. In this study, coking reactions on different-sized Ni catalysts demonstrate that the larger-particle Ni catalyst is more facile for methane decomposition and carbon deposition in a continuous methane flow, due to the formation of encapsulating carbon and whisker carbon (Figs. 6 and 7), and the amount of deposited carbon increases with the Ni particle size (Table 2). However, these results cannot explain the deactivation of larger-particle Ni catalysts in the MATR process, because no carbon deposition was observed on the surface of the deactivated catalysts.

On the other hand, pulse-injected surface reactions of methane at different atmospheric conditions demonstrated that the small-particle Ni catalyst was more effective and stable for methane decomposition and catalytic conversion. The TOF of methane decreased with increasing Ni particle size, and the larger-particle Ni catalyst deactivated continuously with the pulse number in both the CH_4–CO_2 and CH_4–O_2 atmospheres.

The deactivation of the larger-particle Ni catalyst in the CH_4–CO_2 pulse experiment can be attributed to carbon deposition, because part of the carbon derived from methane decomposition is inactive in CO_2 atmosphere. In the O_2–CH_4 atmosphere, the deactivation may have been caused by the Ni that was oxidized due to the slow methane decomposition rate. But the smaller-particle Ni catalyst remained stable during the first 5 pulses in CO_2- and O_2-containing flow. These results indicate that CH_4-TPDe in a continuous methane flow can represent only the tolerance of carbon in different-sized Ni catalysts, whereas there is no clear relationship between carbon tolerance and the detected catalytic activity [32,33]. Because the controlled contact time is short, pulse surface reaction can disclose the CH_4 decomposition rate related to the detected catalyst activity.

4.4. Deactivation of Ni catalysts at higher space velocity

The relative rate of carbon formation (methane decomposition) and its oxidative removal play very important roles in its deactivation. These two steps need to be maintained in a dynamic balance to achieve stable operation. When the former step is faster than the latter, excessive carbon deposition will occur; when the former step is slower than the latter, the metallic Ni particle becomes exposed in the remaining oxygen and oxidized. But this relationship is contradictory in methane dry reforming; the reason for deactivation of the larger-particle Ni catalysts and deactivation at higher space velocity in the MATR process is that the relative rate of carbon formation (methane decomposition) is lower than its oxidative removal. We suppose that the highest space velocity for the stable operation of this oxygen-containing flow should be controlled at a rate of methane decomposition equal to that of the oxidative removal of surface carbons. At this space velocity, oxygen should be consumed completely (and the minimum methane conversion should be kept >60%, because $CH_4/O_2 = 1/0.3$ in feed). Above this space velocity, the relative rate of methane decomposition is lower than its oxidative removal; consequently, the remaining oxygen leads to Ni oxidation and deactivation. This hypothesis could be contributing to the continuous deactivation of the 4.5-nm Ni catalyst at 90,000 h^{-1}. Whereas in our previous work [19,20], the coupled catalytic partial oxidation and steam methane reforming process operated at lower space velocity (<9000 h^{-1}) [34], the reforming reaction is expected to occur simultaneously with the oxidative conversion reaction, and the composition of the product gases is expected to be close to thermodynamic equilibrium. The stability of these catalysts at the lower space velocity (<9000 h^{-1}) does not demonstrate the dynamic balance between methane decomposition and its oxidative removal.

Methane decomposition on the surface of Ni catalyst is very important to prevent oxidation of metallic Ni by O_2 in feed. Thermodynamic analysis has indicated that both carbons deposited on Ni (such as Ni_3C) and free carbons are more reactive toward O_2 than metallic Ni in the reaction conditions (700 °C):

$$Ni_3C + (1/2)O_2 \rightarrow 3Ni + CO, \quad \Delta G_{998K} = -448.4\ \text{kJ/mol}, \tag{7}$$

$$C + (1/2)O_2 \rightarrow CO, \quad \Delta G_{998K} = -197.8\ \text{kJ/mol}, \tag{8}$$

$$Ni + (1/2)O_2 \rightarrow NiO, \quad \Delta G_{998K} = -151.5\ \text{kJ/mol}. \tag{9}$$

Carbons can protect metallic nickel from being oxidized in the O_2-containing flow. When methane decomposition rate is slow on larger-particle Ni at higher space velocities, the amount of formed surface carbon is insufficient to ensure complete conversion of the oxygen added in the feed.

4.5. Deactivation mechanism of Ni catalyst during MATR

According to the above results and discussion, we can characterize the reaction mechanism of MATR and deactivation mechanism of Ni catalysts in the fluidized bed as follows:

(1) Methane first adsorbs and decomposes on the surface of metallic Ni catalysts. The small-particle Ni catalyst is more active and effective for methane decomposition. This step can be expressed as

$$CH_4 + nNi \rightarrow CH_x\text{–}Ni_m + (4-x)H\text{–}Ni \quad (x = 0\text{–}3), \tag{10}$$

$$CH_x\text{–}Ni_m \rightarrow C\text{–}Ni_{m-x} + xH\text{–}Ni, \tag{11}$$

and

$$2H\text{–}Ni \rightarrow H_2 + 2Ni. \tag{12}$$

During methane decomposition, hydrogen releases quickly to the gas phase, but carbon deposits on the surface of Ni catalysts.

(2) Carbon deposited on the surface of Ni catalysts is gasified by O_2 and CO_2:

$$C\text{–}Ni_m + (1/2)O_2 \rightarrow CO + Ni_m \tag{13}$$

and

$$C\text{–}Ni_m + CO_2 \rightarrow 2CO + Ni_m. \tag{14}$$

The highest space velocity for the stable operation of this oxygen-containing flow should be controlled at the rate of methane decomposition equal to that of the oxidative removal of surface carbons. Above this space velocity, metallic Ni particles will be oxidized to NiO [Eq. (9)], and NiO can be readily reduced hydrogen flow,

$$NiO + H_2 \rightarrow Ni + H_2O. \tag{15}$$

(3) On larger Ni particles and/or at higher space velocity, methane decomposition is slower than the oxidative removal of surface carbons, and complete conversion of the oxygen added in the feed cannot be ensured. Surface Ni will be oxidized gradually into NiO by remaining O_2, causing further Ni catalyst deactivation.

5. Conclusion

We found that both the activity and stability of the Ni catalysts depend strongly on the particle size and the operating space velocity in MATR process in a fluidized-bed reactor. The smaller-particle Ni catalyst was more active and stable than

the larger-particle Ni catalyst at space velocity $<54{,}000\ h^{-1}$. Methane activation reactions in various atmospheres demonstrated that the methane decomposition rate decreased with the Ni particle size. When the methane decomposition rate was slow and the amount of formed surface carbon insufficient (on larger Ni particles and/or at higher space velocity) to ensure complete conversion of the oxygen added in the feed, surface Ni was oxidized gradually to NiO by remaining O_2, causing further Ni catalyst deactivation.

Acknowledgments

This project was supported by the National Natural Science Foundation of China (20433030, 90610002) and the Zhejiang Provincial Natural Science Foundation (Z406142).

References

[1] Y.H. Hu, E. Ruckenstein, Adv. Catal. 48 (2004) 297.
[2] S.M. Stagg-Williams, F.B. Noronha, Recent Res. Devel. Catal. 2 (2003) 205.
[3] M. Aresta, ACS Symp. Ser. (Utilization of Greenhouse Gases) 852 (2003) 2.
[4] L. Pinaeva, Y. Schuurman, C. Mirodatos, in: M.M. Maroto-Valer, C.S. Song, Y. Soong (Eds.), Environmental Challenges and Greenhouse Gas Control for Fossil Fuel Utilization in the 21st Century, Proc. 221st National Meet. ACS, San Diego, CA, 1–5 April 2001, Kluwer, New York, 2002, p. 313.
[5] Y.H. Hu, E. Ruckenstein, Catal. Rev. 44 (2002) 423.
[6] R.M. Watwe, H.S. Bengaard, J.R. Rostrup-Nielsen, J.A. Dumesic, J.K. Nørskov, J. Catal. 189 (2000) 16.
[7] H.S. Bengaard, J.K. Nørskov, J. Sehested, B.S. Clausen, L.P. Nielsen, A.M. Molenbroek, J.R. Rostrup-Nielsen, J. Catal. 209 (2002) 365.
[8] E. Ruckenstein, H.Y. Wang, J. Catal. 205 (2002) 289.
[9] M.C.J. Bradford, M.A. Vannice, Catal. Rev. 41 (1999) 1.
[10] V.R. Choudhary, K.C. Mondal, A.S. Mamman, J. Catal. 233 (2005) 36.
[11] K. Tomishige, Catal. Today 89 (2004) 405.
[12] K. Tomishige, Y. Matsuo, Y. Sekine, K. Fujimoto, Catal. Commun. 2 (2001) 11.
[13] Y. Matsuo, Y. Yoshinaga, Y. Sekine, K. Tomishige, K. Fujimoto, Catal. Today 63 (2000) 439.
[14] C.S. Song, W. Pan, Catal. Today 98 (2004) 463.
[15] Q.S. Jing, H. Lou, L.Y. Mo, J.H. Fei, X.M. Zheng, J. Mol. Catal. A 212 (2004) 211.
[16] K. Nagaoka, A. Jentys, J.A. Lercher, J. Catal. 229 (2005) 185.
[17] B.T. Li, K. Maruyama, M. Nurunnabi, K. Kunimori, K. Tomishige, Ind. Eng. Chem. Res. 44 (2005) 485.
[18] B.T. Li, K. Maruyama, M. Nurunnabi, K. Kunimori, K. Tomishige, Appl. Catal. A. 275 (2004) 157.
[19] Q.S. Jing, H. Lou, J.H. Fei, Z.Y. Hou, X.M. Zheng, Int. J. Hydrogen Energy 29 (2004) 1245.
[20] L.Y. Mo, X.M. Zheng, Q.S. Jing, H. Hou, J.H. Fei, Energy Fuels 19 (2005) 49.
[21] M.E. Farago, J.M. James, V.C.G. Trew, J. Chem. Soc. A (1967) 820.
[22] J.Y. Carriat, M. Che, M. Kermarec, M. Verdaguer, A. Michalowicz, J. Am. Chem. Soc. 120 (1998) 2059.
[23] C.M. Cook, F.A. Long, J. Am. Chem. Soc. 73 (1951) 4119.
[24] D. Kunii, O. Levenspiel, Fluidization Engineering, Wiley, New York, 1969, p. 66.
[25] C.N. Triantafyllopoulos, S.G. Neophytides, J. Catal. 239 (2006) 187.
[26] D.L. Trimm, Catal. Today 49 (1999) 3.
[27] Z.Y. Hou, O. Yokota, T. Tanaka, T. Yashima, Appl. Surf. Sci. 233 (2004) 58.
[28] P. Chen, Z.Y. Hou, X.M. Zheng, T. Yashima, React. Kinet. Catal. Lett. 86 (2005) 51.
[29] V.C.H. Kroll, H.M. Swaan, C. Mirodatos, J. Catal. 162 (1996) 409.
[30] M.M.V.M. Souza, M. Schmal, Appl. Catal. A 255 (2003) 83.
[31] G.S. Gallego, F. Mondragon, J. Barrault, J.M. Tatibouet, C. Batiot-Dupeyrat, Appl. Catal. A 311 (2006) 164.
[32] Z.Y. Hou, T. Yashima, Catal. Lett. 89 (2003) 193.
[33] Z.Y. Hou, T. Yashima, Appl. Catal. A 261 (2004) 205.
[34] L.W. Chen, Q. Hong, J.Y. Lin, F.M. Dautzenberg, J. Power Sources 164 (2007) 803.